University of Massachusetts Medical School
eScholarship@UMMS

University of Massachusetts Medical School Faculty Publications

2013-11-27

Amphotericin B increases influenza A virus infection by preventing IFITM3-mediated restriction

Tsai-Yu Lin
University of Massachusetts Medical School

Et al.

Let us know how access to this document benefits you.
Follow this and additional works at: https://escholarship.umassmed.edu/faculty_pubs

 Part of the Immunology of Infectious Disease Commons, Immunopathology Commons, Immunoprophylaxis and Therapy Commons, Influenza Humans Commons, and the Virology Commons

Repository Citation

Lin T, Chin CR, Everitt AR, Clare S, Perreira J, Savidis G, Aker AM, John SP, Sarlah D, Carreira EM, Elledge SJ, Kellam P, Brass AL. (2013). Amphotericin B increases influenza A virus infection by preventing IFITM3-mediated restriction. University of Massachusetts Medical School Faculty Publications. https://doi.org/10.1016/j.celrep.2013.10.033. Retrieved from https://escholarship.umassmed.edu/faculty_pubs/805

Creative Commons License

This work is licensed under a Creative Commons Attribution-Noncommercial-No Derivative Works 3.0 License.
This material is brought to you by eScholarship@UMMS. It has been accepted for inclusion in University of Massachusetts Medical School Faculty Publications by an authorized administrator of eScholarship@UMMS. For more information, please contact Lisa.Palmer@umassmed.edu.

Cell Reports
Report

Cell PRESS
Open ACCESS

Amphotericin B Increases Influenza A Virus Infection by Preventing IFITM3-Mediated Restriction

Tsai-Yu Lin,[1,9] Christopher R. Chin,[1,2,9] Aaron R. Everitt,[3] Simon Clare,[3] Jill M. Perreira,[1] George Savidis,[1] Aaron M. Aker,[1] Sinu P. John,[2] David Sarlah,[4] Erick M. Carreira,[4] Stephen J. Elledge,[5,6,7] Paul Kellam,[3,8] and Abraham L. Brass[1,2,10,*]
[1]Department of Microbiology and Physiological Systems, University of Massachusetts Medical School, Worcester, MA 01655, USA
[2]Ragon Institute of Massachusetts General Hospital, M.I.T. and Harvard University, Charlestown, MA 02129, USA
[3]Wellcome Trust Sanger Institute, Wellcome Trust Genome Campus, Hinxton CB10 1SA, UK
[4]Eidgenössische Technische Hochschule, Deutsch English Department of Chemistry and Applied Biosciences, 8093 Zurich, Switzerland
[5]Department of Genetics, Harvard Medical School, 77 Avenue Louis Pasteur, Boston, MA 02115, USA
[6]Division of Genetics, Brigham and Women's Hospital, 77 Avenue Louis Pasteur, Boston, MA 02115, USA
[7]Howard Hughes Medical Institute, 4000 Jones Bridge Road, Chevy Chase, MD 20815, USA
[8]MRC/UCL Centre for Medical Molecular Virology, Division of Infection & Immunity, University College London, Gower Street, London W1CE 6BT, UK
[9]These authors contributed equally to this work
[10]Present address: Department of Microbiology and Physiological Systems, University of Massachusetts Medical School, Albert Sherman Center, 368 Plantation Street, 8 1001, Worcester, MA 01655, USA
*Correspondence: abraham.brass@umassmed.edu
http://dx.doi.org/10.1016/j.celrep.2013.10.033
This is an open-access article distributed under the terms of the Creative Commons Attribution-NonCommercial-No Derivative Works License, which permits non-commercial use, distribution, and reproduction in any medium, provided the original author and source are credited.

SUMMARY

The IFITMs inhibit influenza A virus (IAV) replication in vitro and in vivo. Here, we establish that the antimycotic heptaen, amphotericin B (AmphoB), prevents IFITM3-mediated restriction of IAV, thereby increasing viral replication. Consistent with its neutralization of IFITM3, a clinical preparation of AmphoB, AmBisome, reduces the majority of interferon's protective effect against IAV in vitro. Mechanistic studies reveal that IFITM1 decreases host-membrane fluidity, suggesting both a possible mechanism for IFITM-mediated restriction and its negation by AmphoB. Notably, we reveal that mice treated with AmBisome succumbed to a normally mild IAV infection, similar to animals deficient in Ifitm3. Therefore, patients receiving antifungal therapy with clinical preparations of AmphoB may be functionally immunocompromised and thus more vulnerable to influenza, as well as other IFITM3-restricted viral infections.

INTRODUCTION

Influenza epidemics perennially result in significant morbidity and mortality, with immunocompromised populations being at particularly high risk. During IAV infection, the viral hemagglutinin (HA) proteins bind to host cell receptors. Upon endocytosis and endosomal acidification, the HA protein undergoes a conformational change leading to fusion of the viral and host membranes. Viral ribonucleoproteins (vRNPs) then enter the cytosol and translocate to the nucleus to commence replication (Medina and García-Sastre, 2011).

IFITM1, IFITM2, and IFITM3 comprise a family of restriction factors that possess broad antiviral activities (Brass et al., 2009; Jiang et al., 2010; Mudhasani et al., 2013). IFITM3 is most active against IAV and resides in late endosomes and lysosomes, while IFITM1 is located on the cell surface and blocks hepatitis C virus (HCV) and the filoviruses Ebola and Marburg (Feeley et al., 2011; Huang et al., 2011; Wilkins et al., 2013). The IFITM proteins are members of the CD225 protein superfamily and contain two intramembrane domains (IM1 and IM2), which traverse through the cytosolic-facing leaflet of the lipid bilayer and are joined by a conserved intracellular loop (Yount et al., 2012). IFITM3 plays a critical role in vivo because *Ifitm3*$^{-/-}$ mice succumb to a normally mild IAV infection (Bailey et al., 2012; Everitt et al., 2012). Furthermore, individuals with a variant of IFITM3 are more likely to suffer a worse course of influenza (Everitt et al., 2012; Zhang et al., 2013). IFITM3 accounts for 50% to 80% of the in vitro protective effects of interferon (IFN) against IAV and blocks viral particle fusion subsequent to endocytosis, thereby preventing the cytosolic entry and nuclear translocation of vRNPs (Feeley et al., 2011; Huang et al., 2011; Weidner et al., 2010). The IFITMs thus represent a restriction factor family of growing translational importance that protects the host at the earliest stages of infection (Diamond and Farzan, 2013; Perreira et al., 2013).

Several efforts have recently investigated the mechanism of IFITM-mediated restriction. For example, it has been reported that the IFITMs decrease membrane fluidity and block viral-envelope-induced hemifusion, the latter conclusion predicated on the alleviation of an IFITM block to cell-to-cell fusion by oleic acid (Li et al., 2013). Moreover, it has been postulated that the IFITMs inhibit VSV-g-mediated fusion by disrupting normal lipid

trafficking, resulting in elevated levels of cholesterol in the late endosomal and lysosomal membranes (Amini-Bavil-Olyaee et al., 2013). This last observation may arise from a direct interaction between the IM2 domains of IFITM1, IFITM2, and IFITM3 and the endocytic trafficking protein vesicle-associated membrane protein A (VAPA). IFITM binding to VAPA may interfere with the interaction of VAPA with oxysterol binding protein (OSBP), a known regulator of cholesterol trafficking (Wyles et al., 2002). Therefore, IFITMs are envisioned to compete with OSBP for binding to VAPA, producing elevated levels of cholesterol that block viral fusion.

While treating fungal infection of our tissue culture cells with the antimycotic AmphoB we noticed that the previous differences in the levels of IAV infection due to differing levels of IFITM3 were surprisingly erased. AmphoB has been used to treat systemic fungal infections, including Aspergillosis, since the 1950's, and its clinical formulations are currently used widely to treat a growing number of such cases (Bellmann, 2007). AmphoB's mechanism of action is thought to involve its binding to the fungal membrane constituent, ergosterol, leading to pore formation and ion egress (Bolard, 1986). In the clinic, AmphoB treatment produces severe side effects because of the formation of such membrane-spanning pores, which increase in diameter as a function of concentration, with low concentrations (0.1 μM) permitting Na^+ and K^+ to traverse and higher levels (>5 μM) allowing the passage of larger cations (e.g., Ca^{+2} and H_3O^+). To overcome this toxicity, two liposomal preparations of AmphoB, AmBisome and Abelcet, were developed, both of which manifest reduced side effects by preferentially targeting fungal membranes. AmBisome is thus a first-line therapy for systemic fungal infections with an estimated $330 million in annual sales worldwide (Moen et al., 2009). Of note, after commencement of our investigations, AmphoB was reported to increase IAV replication in vitro; however, both the mechanism and the in vivo implications of this phenomenon remain obscure (Roethl et al., 2011). Therefore, intrigued by our observations regarding IFITM3's neutralization by AmphoB, we pursued studies to elucidate both the mechanism of this interaction and its potential in vivo consequences.

RESULTS

To investigate our observations regarding AmphoB and IFITM3, we first evaluated the effect of AmphoB on IAV replication in IFITM-depleted cells. HeLa cervical adenocarcinoma cells were stably transduced with either of two short hairpin RNAs (shRNAs) targeting IFITM3 or two negative control shRNAs against firefly luciferase (Figures 1A and 1B). HeLa cells were chosen because they express relatively high levels of endogenous IFITM3 and differing endogenous levels of IFITM3 strongly correlate with AmphoB's effects on IAV replication (Feeley et al., 2011; Roethl et al., 2011). The cell lines were then challenged with either of two strains of IAV, H1N1 A/WSN/33 (WSN/33) or H1N1 A/PR/38 (PR8), with or without AmphoB. The loss of IFITM3 in untreated cells increased the infection of both viruses, with the enhancement being greater for PR8 (25-fold) than for WSN/33 (5-fold). In the IFITM3-depleted cells treated with AmphoB, we saw no increased infection with WSN/33 and a modest additional increase in replication with PR8 (1.7- and 2.4-fold, respectively), suggesting that the majority of AmphoB's enhancement of IAV infection is due to overcoming IFITM3. The IFITMs act on the viral envelope protein-dependent stage of entry by blocking fusion. Therefore, we tested the effect of AmphoB on the infectivity of viral pseudoparticles that express the HA1, HA5, or HA7 proteins. Consistent with its overcoming IFITM3, AmphoB treatment enhanced the infectivity of all of the HA-expressing particles (Figure 1C). Notably, the infectivity of particles bearing PR8's HA1 was uniquely increased in the vector cells treated with AmphoB, suggesting that the residual infectivity seen when IAV PR8 is used with IFITM3-depleted cells (Figure 1A) is the result of an intrinsic property of the PR8 HA1 envelope. Interestingly, while IFITM3 did modestly inhibit VSV-g pseudoparticle infection, this block was not alleviated by AmphoB.

We next tested A549 human lung carcinoma cells expressing high levels of exogenous IFITM3 and observed that AmphoB (1 μM) produced a marked reversal of IFITM3-mediated restriction at both 12 and 24 hr postinfection (Figure 1D; Figures S1A–S1D). Similar results were seen with influenza B virus (data not shown). Due to decreased toxicity, liposomal preparations of AmphoB (AmBisome) are used to treat patients with fungal infections. Therefore, we investigated if AmBisome also rescued IAV infection from IFITM3. This was the case, as AmBisome's effect on IFITM3-mediated restriction was indistinguishable from that of AmphoB at a clinically relevant concentration (2 μM; Figure 1E). Notably, therapeutically administered maximal concentrations of AmphoB and AmBisome range from 1 to 3 μM (Bellmann, 2007). Given IFITM3's role in the IFN response, we determined the effect of AmBisome on IFN-α-induced restriction of IAV (Figure 1F). IFN-α inhibited IAV infection in both the vector and IFITM3 cells, with the addition of AmBisome rescuing >60% of IAV infectivity, consistent with the 60%–80% of the IFN response that is lost with IFITM3 depletion (Brass et al., 2009). Thus, AmBisome removes the majority of IFN's protection from IAV in vitro.

A basic amine in the mycosamine of AmphoB is critical for its antimycotic activity (Volmer and Carreira, 2010). This amine is protonated at physiological pH and makes key interactions with the lipid bilayer. Consequently, we synthesized DS-AmpB-020, which incorporates additional cationic sites at the mycosamine (Figure 1G). Indeed, this compound displays 15-fold more antifungal activity (Paquet et al., 2008). Treatment of A549-IFITM3 cells with DS-AmpB-020 resulted in the complete loss of IFITM3-mediated restriction and showed this compound to be more potent than AmphoB (4-fold lower IC_{50}; Figure 1H). Together, these data suggest that the chemical moieties required for the antifungal properties of these compounds are also important for their alleviation of IFITM3's antiviral actions.

IFITM3 blocks IAV fusion and prevents vRNPs from translocating to the nucleus (Feeley et al., 2011). We examined the effect of AmphoB on IAV vRNP nuclear translocation (Figure 2A). At the start of infection, the IAV nucleoprotein (NP) is associated with the vRNPs. By immunostaining for NP, we can follow vRNP distribution intracellularly. HeLa-vector or HeLa-IFITM3 cells were chilled on ice with IAV PR8. Next, the viral supernatant was

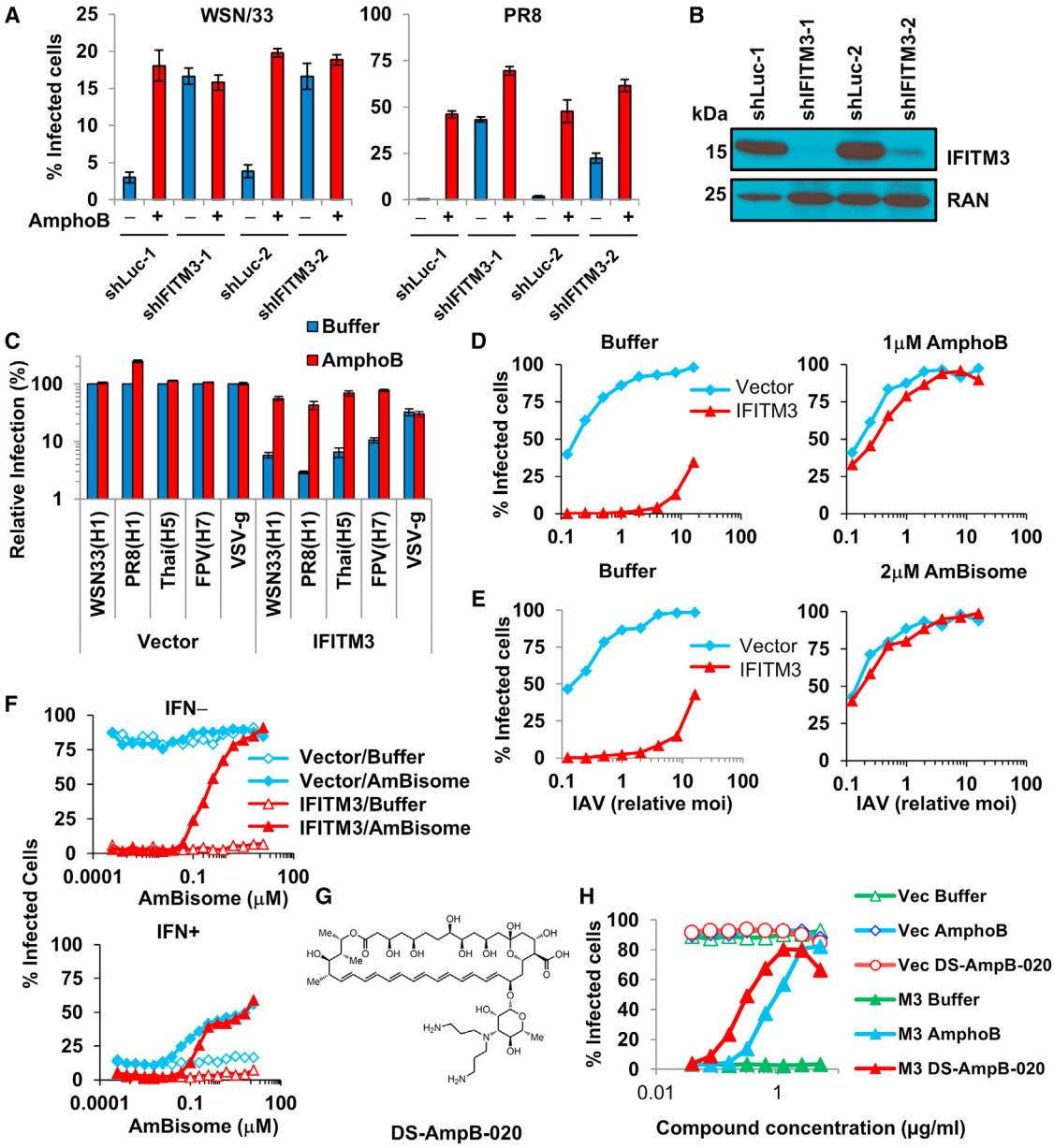

Figure 1. AmphoB Increases IAV Infection by Preventing IFITM3-Mediated Restriction In Vitro

(A) HeLa cells stably expressing either of two negative control short hairpin RNAs (shRNAs) against the firefly luciferase gene (shLuc-1 or shLuc-2) or shRNAs against IFITM3 (shIFITM3-1 and shIFITM3-2) were incubated for 1 hr in the presence (red) or absence (blue) of 1 μM AmphoB, then challenged with IAV WSN/33 (multiplicity of infection [moi] 0.2) or PR8 (moi 0.02) followed by immunostaining for HA. Numbers represent the mean percentage of infected cells of three separate experiments ± SD, as determined by imaging analysis software.

(B) Whole cell lysates from the indicated cells in (A) were subjected to immunoblotting using the noted antibodies. kDa, kilodaltons. RAN serves as a loading control.

(C) IFITM3's restriction of HA-mediated entry is overcome by AmphoB. A549 cells stably transduced with IFITM3 or with vector alone (Vector) were treated with 1 μM AmphoB (red) or buffer (blue) then challenged with the indicated pseudotyped MLV-GFP particles: WSN/33 (H1), PR8 (H1), Thai (H5), FPV (H7), or the g protein of VSV. Relative infection represents the percentage of GFP-positive cells normalized to that of A549-vector cells as determined by fluorescence-based imaging. Results are the mean of three independent experiments ± SD.

(D and E) A549-vector (blue) or A549-IFITM3 (red) cells were infected with increasing amounts of IAV (WSN/33, relative moi) in the presence or absence of AmphoB (D) or AmBisome (E). Infectivity was determined by immunostaining for surface HA protein.

(F) IAV infection (WSN/33, moi 2) of A549-vector (blue) or A549-IFITM3 (red) cells in the presence (closed symbols) or absence (open symbols) of AmBisome or IFN-α.

(G) Structure of the AmphoB derivative DS-AmpB-020.

(H) A549-vector (Vec, open symbols) or -IFITM3 (M3, closed symbols) cells were infected with IAV (WSN/33, moi 2) in the absence (buffer, green lines) or presence of increasing concentrations of either AmphoB (blue) or DS-AmpB-020 (red).

Results are representative of three independent experiments.

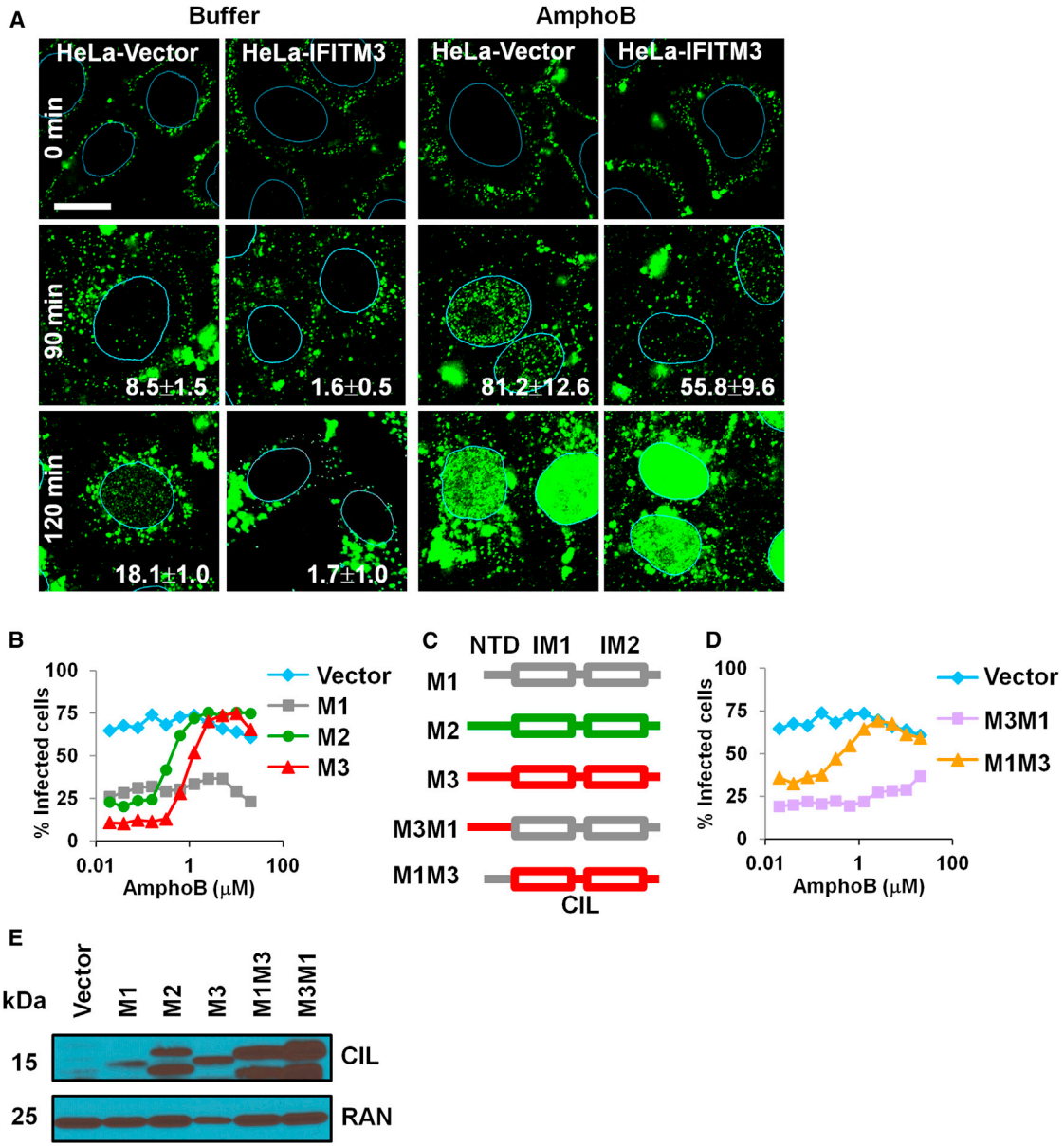

Figure 2. AmphoB Prevents IFITM2- and IFITM3-Mediated Restriction, but Not Restriction by IFITM1

(A) HeLa-vector or HeLa-IFITM3 cells were incubated with AmphoB or buffer for 1 hr prior to being incubated on ice with IAV PR8. Warm media was added at time zero. Cells were fixed at the indicated time points, immunostained for the IAV NP protein (green) and stained for DNA, then analyzed by confocal microscopy. Image analysis software was used to define each cell's nuclear peripheries (blue lines based on the staining of nuclear DNA). Numbers represent the number of NP particles (green) present per nucleus at the indicated time points and are the mean ± SD of three independent experiments. Scale bar, 10 μM.

(B) A549 cells stably transduced with vector alone (Vector) or with IFITM1 (M1), IFITM2 (M2), or IFITM3 (M3) were incubated for 1 hr with increasing concentrations of AmphoB followed by infection with IAV WSN/33 for 12 hr and immunostaining for HA.

(C) Schematic diagram of the IFITM chimeras. The N- and C-terminal domains (NTD, CTD) and intramembrane domains 1 and 2 (IM1 and IM2) are shown, separated by the conserved intracellular loop (CIL). M1, IFITM1 (gray); M2, IFITM2 (green); M3, IFITM3 (red). The chimeric proteins (M3M1 and M1M3) are shown below, with the first M# representing the NTD's origins and the second M# denoting the consignation of the remaining portion of the protein.

(D) A549 cells stably transduced with vector alone (Vector) or the indicated chimeras were incubated for 1 hr with increasing concentrations of AmphoB prior to infection with IAV WSN/33 as above.

(E) Immunoblot of the indicated cell lines using the CIL antisera, which recognizes an epitope that is identical across all of the IFITM WT proteins and chimeras. Results are representative of three independent experiments.

replaced with warm media (0 min). At the indicated times after warming, cells were evaluated for NP signal with a confocal microscope. vRNPs arrive in the nuclei by 90 min in the vector cells, with the NP signal increasing through to 120 min, and these events are inhibited by IFITM3 overexpression. Remarkably, when we treated the cell lines with AmphoB, both the vector and IFITM3 cells showed a strong increase in vRNP particles in their nuclei, although the vector cells were still more infected at 90 min. A time of addition experiment showed that AmphoB's effect was maximal when added 60 min prior to viral addition, consistent with inhibiting IFITM3 (Figure S1E). An immunoblot revealed that AmphoB treatment did not decrease IFITM3 levels (Figure S1F). Together with the pseudoparticle experiments, these data demonstrate that AmphoB's enhancement of IAV infection arises from it overcoming IFITM3's inhibition of viral fusion.

To determine the specificity of AmphoB's actions, we compared its effect on A549 cells stably expressing IFITM1, IFITM2, or IFITM3. These experiments showed that while AmphoB effectively counteracts IFITM2 and IFITM3, its neutralization of IFITM1 was considerably less, with only a 1.4-fold increase in infection observed (Figure 2B). Next, chimeric IFITM proteins were constructed to find what regions of IFITM3 confer AmphoB sensitivity (John et al., 2013). IFITM3's N-terminal domain (NTD) was fused with the remaining portions of IFITM1 to generate M3M1, and the NTD of IFITM1 was fused to IFITM3 to produce M1M3 (Figure 2C). The M3M1 chimera was less affected by AmphoB treatment similar to wild-type (WT) IFITM1, and the M1M3 protein was rendered ineffective by AmphoB (Figure 2D). The levels of the WT IFITM proteins in the cell lines used for these experiments were purposefully matched to the expression levels of the chimeras, resulting in less restriction than seen with higher-expressing cell lines (Figure 2E). These results reveal that AmphoB impacts IFITM2 and IFITM3 greater than IFITM1 and that this susceptibility resides in amino acids 51–133 of IFITM3.

IFITM3's mechanism of restriction is not fully understood. Given that AmphoB reverses IFITM3's inhibition of viral replication, we set about using it as a molecular probe to investigate IFITM3's actions. IAV fusion requires endosomal acidification, and IFITM3 both blocks IAV fusion and increases intracellular acidity by expanding the late endosomal and lysosomal compartments (Feeley et al., 2011). Therefore, IFITM3 might inhibit IAV by altering endosomal pH. To test this idea, HeLa-vector and HeLa-IFITM3 cells were stably transduced with a RAB7-red fluorescent protein (RAB7-RFP) to identify their late endosomes and lysosomes. The cell lines were then incubated with a mixture of two dextrans, conjugated to either a pH-sensitive or pH-insensitive fluor, in the presence or absence of AmphoB. Calculating the ratio of these two signals allowed us to determine that IFITM3 increased the acidity in the RAB7 compartments (Figure S2A). In addition, AmphoB modestly decreased the relative acidity of both the vector and IFITM3 cell lines. We next evaluated the consequences of AmphoB's altering pH on acid-induced HA activation. At the indicated times after the initiation of a synchronized infection, we immunostained for the presence of HA that has undergone an acid-induced conformational change required for fusion (Figure S2B). These experiments showed more acid-induced HA signal in the IFITM3 cells, consistent with their higher acidity. However, we observed no appreciable change in the levels of acid-induced HA upon AmphoB treatment of either cell line. Along with the dextran and NP translocation studies, these results suggest that AmphoB did not prevent IFITM3-mediated restriction by decreasing endosomal acidity. These studies also showed that the levels and location of IFITM3 were not altered by AmphoB treatment with or without viral infection.

AmphoB's pores permit the diffusion of ions across membranes (Bolard, 1986). Endosomal membrane potential and ion concentration (Na^+, K^+, and Cl^-) play roles in both endocytosis and viral-host membrane fusion (Helenius et al., 1985; Scott and Gruenberg, 2011). Therefore, we examined how IFITM3 and AmphoB influence endosomal Na^+ levels. Vector and IFITM3 cells were treated with AmphoB, nystatin (a related heptaen), or three Na^+ ionophores, then incubated with a cell-impermeable fluorescent indicator, Asante Na^+ green 2 (ANG-2). ANG-2 remains in the endocytic compartment permitting the visualization of Na^+ levels in vital endosomes. The HeLa-IFITM3 cells showed a higher ANG-2 signal than vector (normalized maximum ANG-2 intensity of IFITM3 cells = 1.28, vector = 1.0; p value = 2.2×10^{-5}; Figure 3A), indicating that IFITM3 increases endosomal salinity as well as acidity. Addition of the indicated compounds after ANG-2 reduced the intensity of the Na^+ signal in both cell lines. However, the loss of IFITM3-mediated restriction was seen only with AmphoB or nystatin treatment and not with any of the ionophores (Figure 3B). Therefore, AmphoB's diminishment of endosomal Na^+ concentration alone is unlikely to explain its counteracting IFITM3-mediated restriction.

Nystatin, a pore-forming heptaen like AmphoB, was the only other compound found to rescue IAV infection from IFITM3. In contrast, the ionophores do not form pores but instead transport Na^+ by encasing the ion and shuttling it across the bilayer (Figure 3C). This difference suggests that egress of a combination of ions (Cybulska et al., 1995; Hartsel et al., 1994), or the pore itself may alter the membrane's properties and underlie AmphoB's negation of IFITM3. To investigate this, we used two small molecules, tetraethylammonium (TEA) and acetylcholine (ACh), to block AmphoB pores (Brutyan and McPhie, 1996; Terazima and Yoshino, 2010; Figure 3C). We first determined conditions where TEA or ACh prevented the AmphoB-mediated efflux of Na^+ from endosomes (Figure 3D; quantitation provided in Figure S2C). Importantly, we assume from these results that the diffusion of additional ions (i.e., K^+ and Cl^-) through the AmphoB pores is also blocked. In support of this, TEA also diminished the modest change in endosomal acidity observed with the addition of AmphoB (Figures S2A and S2D). Next, using these conditions, we challenged the vector and IFITM3 cells with IAV and found that the blockade of AmphoB pores with either TEA or ACh had no effect on AmphoB's rescue of IAV replication (Figure 3E), arguing that alteration of endosomal ion concentration and pore conductance cannot account for either IFITM3-mediated restriction or its negation by AmphoB.

Because AmphoB binds cholesterol and overcomes IFITM3-mediated restriction, we were intrigued by recent studies regarding the IFITMs and VAPA, cholesterol, and oleic acid; therefore, we tested the role of these factors in IFITM3-mediated

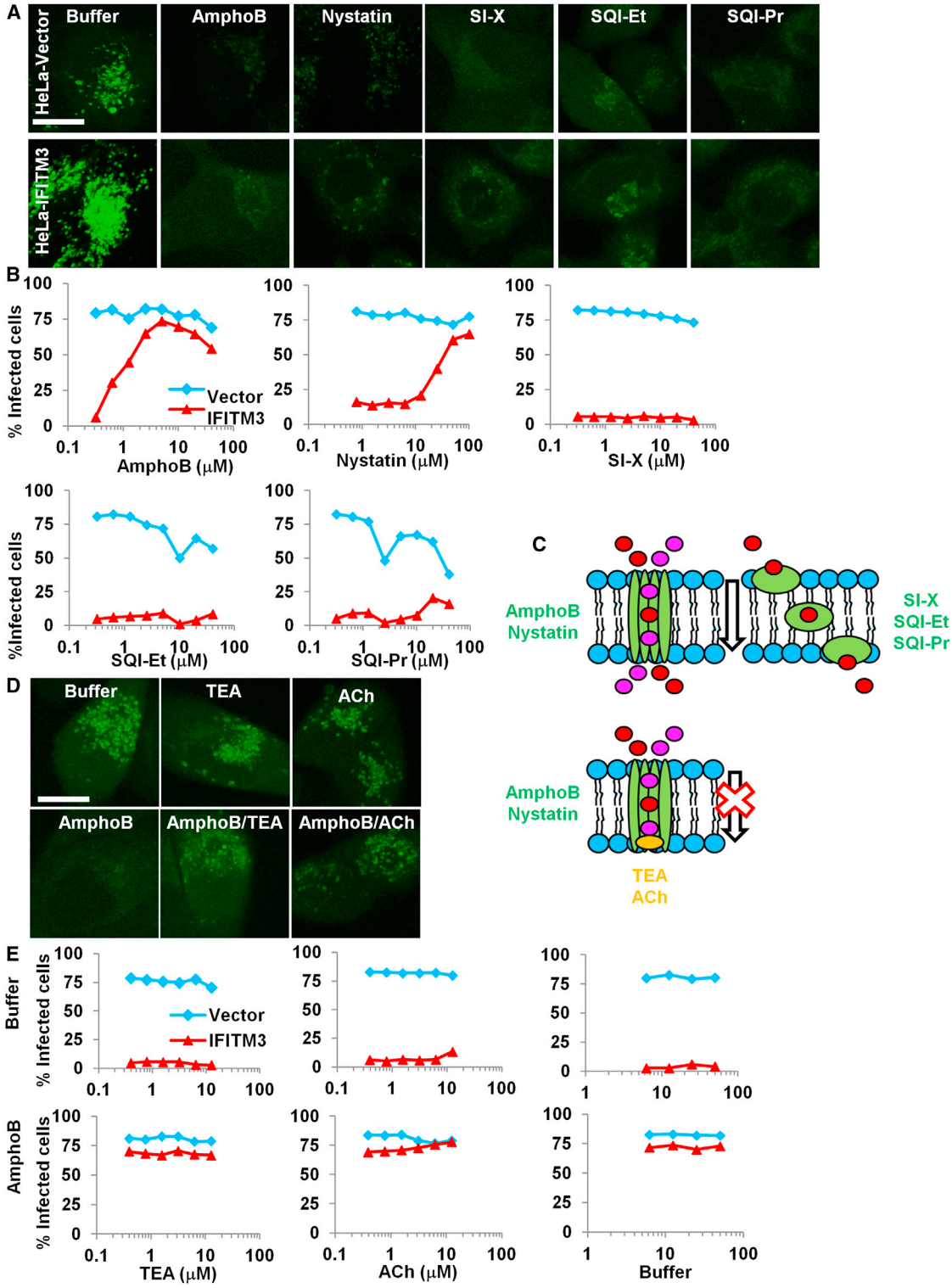

Figure 3. IFITM3's Inhibition of IAV Is Overcome by AmphoB and Nystatin, but Not by Na^+ Ionophores

(A) HeLa-vector or HeLa-IFITM3 cells were incubated with the indicated compounds and stained for endosomal sodium with the fluorescent indicator dye Asante Na^+ green 2 (ANG-2, green) and then imaged using confocal microscopy. The concentrations used were AmphoB 1 μM, nystatin 50 μM, and SI-X, SQI-Et, SQI-Pr 5 μM. Scale bar, 10 μm.

(B) IAV WSN/33 infection (moi = 2) of A549-vector (blue) or A549-IFITM3 (red) cells in the presence or absence of increasing concentrations of the indicated compounds. Cells were treated with the indicated compounds for 1 hr prior to infection.

(legend continued on next page)

inhibition of IAV infection. Confocal imaging using the cholesterol-binding fluorescent probe filipin confirmed that overexpression of either IFITM1 or IFITM3 increased intracellular cholesterol (Figures S3A–S3C; Amini-Bavil-Olyaee et al., 2013). However, lowering the levels of intracellular cholesterol in A549 cells using methyl-β-cyclodextrin (MβCD) or lovastatin resulted in no appreciable difference in restriction of IAV WSN/33 by IFITM1 or IFITM3, with or without AmphoB treatment (Figure 4A). The addition of cholesterol slightly decreased infection in the vector cells and halved AmphoB's alleviation of IFITM3-mediated restriction, although we cannot rule out that the latter result occurs because excess cholesterol prevents AmphoB from reaching an effective intracellular concentration. Notably, treatment of the A549 cell lines with oleic acid had no effect on either IFITM1- or IFITM3-mediated restriction of IAV WSN/33 (Figure 4B). Overexpression of both VAPA and IFITM3 in A549 cells, or VAPA alone in HeLa cells, generated a modest alleviation of IFITM3-mediated restriction of either IAV PR8 or IAV WSN/33 infection (Figures 4D–4F). Neiman-Pick type c1 fibroblasts contain a mutation that results in high levels of cholesterol in late endosomal and lysosomal membranes, but this characteristic did not diminish IAV WSN/33 infection (Figures 4G and 4H; Amini-Bavil-Olyaee et al., 2013). Last, three alanine scan (AS) mutant A549 proteins, each possessing six contiguous residues changed to alanine collectively spanning the IM2 region of IFITM3 that interacts with VAPA, had no loss in restriction compared to WT IFITM3, nor did their respective mutations result in any alterations in lysosomal cholesterol levels (Figures S3D–S3G; John et al., 2013). These data suggest that neither VAPA nor cholesterol nor the alleviation of a block to hemifusion by oleic acid plays a substantial role in either IFITM3-mediated restriction of IAV or its reversal by AmphoB.

The IFITM proteins can associate to form homo- and heteromeric complexes via their IM1 domains, and this interaction is required for restriction of IAV (John et al., 2013). This prompted us to hypothesize that the multimerization of IFITM proteins inhibits viral fusion by altering the fluidity of the cell membrane. To test this idea, we measured the membrane fluidity of cells stably expressing IFITM1 using fluorescence recovery after photobleaching (FRAP). We chose to use COS-7 cells stably transduced with IFITM1 due to their planar morphology and because IFITM1 is predominantly cell-surface expressed as compared to IFITM3, which resides in late endosomes and lysosomes that were not amenable to FRAP studies due to their small size and continued movements (data not shown; Figure 5A; Figure S4A). Caveolin 1 (CAV1) was chosen as a control because it has a similar intramembrane topology to the IFITMs (Hoop et al., 2012; Yount et al., 2012). After incubating the cells along with a fluorescent membrane probe (DiO), we then photobleached an area of the cell surface (white squares, Figure 5B). We monitored the return of the DiO signal as readout for membrane fluidity by capturing serial images of the bleached areas (Figure 5C). These experiments showed that IFITM1 decreased membrane fluidity compared to vector cells, signified by the slower recovery and a greater than 2-fold increase in the immobile fraction in the IFITM1 cells (Figure 5D). Consistent with previous reports, and in contrast to IFITM1, CAV1 expression increased membrane fluidity, demonstrating the specificity of IFITM1's actions (Cai et al., 2004). To test for a functional effect, we emulated elegant studies that established that IAV and other fusogenic viruses can induce tissue culture cells to form syncytia when exposed to low pH (White et al., 1981, 1982). We incubated the COS-7 cell lines (vector, IFITM1, and IFITM3) with concentrated IAV PR8 on ice, followed by the addition of warm buffer at either pH 5.0 or 7.5. After replacing the buffer with media, we stained the cells for actin and DNA followed by image analysis. Quantitation of syncytia, based on clustering of nuclei and the absence of intervening bands of actin (Figure 5E), showed there were less fusion events occurring among the IFITM1 cells (1.5% ± 0.4% fused cells) as compared to either the IFITM3 cells or the vector control cells (3.6% ± 0.6% fused cells, $p < 0.05$; Figures 5F and 5G). We interpret the lack of effect by IFITM3 in this assay to be attributable to its location in the late endosomes and lysosomes. The levels of the exogenously expressed IFITM1 and IFITM3 proteins were seen to be comparable by immunoblotting (Figure 5H). AmphoB did not alter either IFITM1's effect on membrane fluidity or its antifusion actions (Figures S4B and S4C), although this was not altogether unexpected given AmphoB's weak effect on IFITM1-mediated restriction. Therefore, we conclude that IFITM1 decreases membrane fluidity along with increasing resistance to IAV-induced cell-to-cell fusion.

Our data demonstrate that AmphoB increases IAV replication by overcoming IFITM3's protective effects in vitro. To determine the effects of AmphoB on IAV in vivo, we infected either WT or *Ifitm3* knockout mice (*Ifitm3*$^{-/-}$) with a low-pathogenicity strain of IAV (A/X-31 H3N2 [X-31]; (Everitt et al., 2012). At the dose used, the X-31 strain produced a mild illness from which the WT mice made a full recovery (Figures 6A and 6B). In contrast, and consistent with our previous studies, the infected *Ifitm3*$^{-/-}$ mice lost >25% of their body weight with signs of significant illness 6 days postinfection. Notably, WT littermates treated with AmBisome (3 mg/kg injected at days 0, 2, and 4 relative to viral inoculation) behaved identically to the *Ifitm3*$^{-/-}$ mice, experiencing a clinical course usually observed with more pathogenic strains of IAV and manifest by severe symptoms in conjunction with a weight loss exceeding 25% of their starting values. We saw no signs of illness with AmBisome treatment alone in the absence of infection (Figure S5). Evaluation of lung

(C) Schematic diagram of AmphoB or nystatin transmembrane pores (left) permitting the passive diffusion of multiple monovalent cations (purple and red ovals) across the endosomal membrane (arrow indicates high to low concentration gradient). In comparison, the ionophores selectively bind Na^+ (red ovals) in a central region, effectively shielding the positive charge from the hydrophobic interior of the membrane and thus allowing the cation to be transported down the gradient. Adding TEA or ACh blocks the opening of the AmphoB pore, preventing ion transport (lower panel, gold oval).

(D) Confocal images of the relative levels of endosomal sodium based on the fluorescent signal of ANG-2 (green) in A549-vector or A549-IFITM3 cells with or without treatment with AmphoB, TEA, or ACh. Quantitation provided in Figure S2C. Scale bar, 10 μm.

(E) IAV WSN/33 infection of A549-vector (blue) or A549-IFITM3 (red) cells in the presence or absence of AmphoB, TEA, or ACh. Serial dilutions of TEA or ACh were added to cells 1 hr prior to infection. Results are representative of three independent experiments throughout.

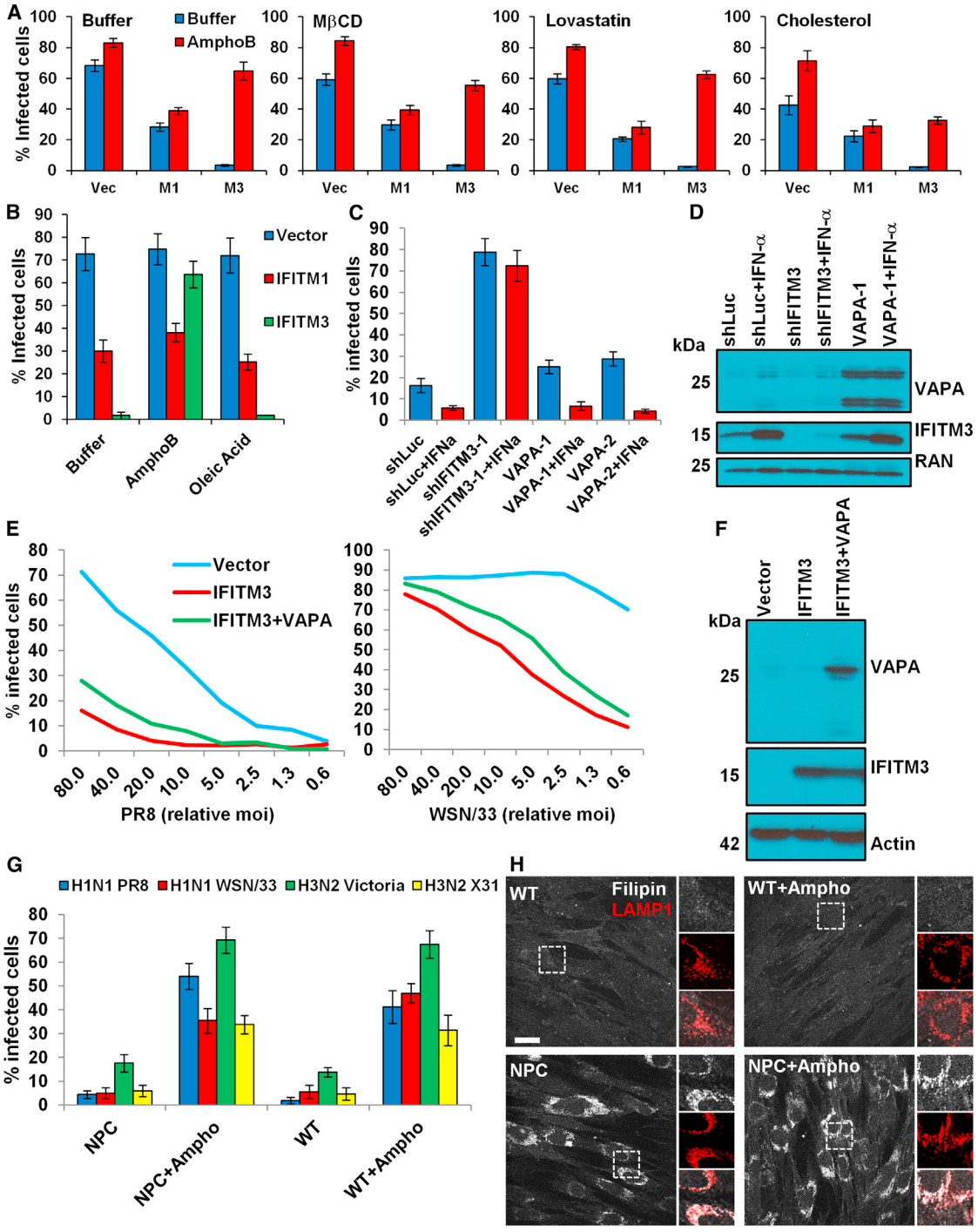

Figure 4. Role of Cholesterol or VAPA in IFITM-Mediated Restriction of IAV

(A) IAV WSN/33 infection (moi 1) of A549-vector (Vec), A549-IFITM1 (M1), or A549-IFITM3 (M3) cells, treated with the indicated small molecules, in the absence (Buffer, blue) or presence of AmphoB (1 μM, red).

(B) IAV WSN/33 infection of A549-vector (blue), A549-IFITM1 (red), or A549-IFITM3 (green) cells treated with the indicated compounds prior to infection.

(C) HeLa cells were stably transduced with retroviruses expressing either a negative control shRNA against the firefly luciferase gene (shLuc-1), a shRNA against IFITM3 (shIFITM3-1), or the VAPA cDNA (for the latter, two independently derived polyclonal cell populations, VAPA-1 and VAPA-2, are shown). Cells were then treated with (red) or without IFN-α (blue) for 16 hr and then infected with IAV WSN/33. Results represent the mean of three independent experiments ± SD.

(D) Whole cell lysates from the indicated cells in (C) were subjected to immunoblotting using the indicated antibodies. RAN serves as a loading control.

(E) Infection of A549-vector (blue), A549-IFITM3 (red), or A549-IFITM3+VAPA (green) cells with increasing amounts of IAV PR8 (left) or IAV WSN/33 (right). Results are representative of three independent experiments.

(legend continued on next page)

pathology at day 6 postinfection showed marked edema, pneumonia, and hemorrhage with substantial inflammation in the AmBisome-treated infected mice (either WT or *Ifitm3*$^{-/-}$) as compared to the WT mice not exposed to AmBisome (Figure 6C). Indeed, in the setting of infection, there is little difference seen when comparing the AmBisome-treated WT lungs to ones from an *Ifitm3*$^{-/-}$ animal.

Consistent with these results, mouse embryonic fibroblasts (MEFs) derived from *Ifitm3*$^{-/-}$ mice were more susceptible to infection than WT MEFs, and this difference was largely erased with AmphoB exposure (Figure 6D, E). Similar to above, the *Ifitm3*$^{-/-}$ cells treated with AmphoB demonstrated a slightly increased infection with X-31, suggesting that Ifitm2 or an additional component is also being overcome by AmphoB. We conclude that a clinical formulation of AmphoB, AmBisome, produces the functional equivalent of an Ifitm3-null state, and by so doing converts a mild illness into a life-threatening infection.

DISCUSSION

We began this study with the observation that treating cells with AmphoB prevented IFITM3-mediated restriction. Upon investigating this phenomenon, we found that overcoming IFITM3 is a principal component of AmphoB-enhanced IAV infection, both confirming and significantly extending a previous study reported during this investigation (Roethl et al., 2011). Of consequence, we also showed that by neutralizing IFITM3's block to viral fusion, AmphoB removed more than 60% of IFN's protective effects against IAV in vitro.

We also used AmphoB as a molecular probe to investigate the mechanism of IFITM3-mediated restriction and determined that while IFITM3 increases both endosomal acidity and salinity, these events are unlikely to play major roles in restriction. Instead, these properties may all arise from the same mechanism, specifically that IFITMs alter the physical properties of membranes. In support of this idea, we determined that IFITM1 decreases membrane fluidity and that this event is associated with inhibition of IAV-induced cell-to-cell fusion; these data are consistent with those recently generated using orthologous approaches (Li et al., 2013). Collectively, these findings have several implications. First, by decreasing membrane fluidity, IFITMs may impede the sequential assembly of viral-host receptor complexes, thereby blocking viral entry. Viruses that rely on multiple receptors for entry would be susceptible to this effect (e.g., HCV and HIV-1). Consistent with this, IFITM1 inhibits both HCV and HIV-1 (Schoggins et al., 2011; Wilkins et al., 2013), and a separate study has reported that the restricted mobility of one of the two HIV-1 host receptors, CD4, can inhibit viral fusion (Rawat et al., 2008). Similarly, recent work has elegantly shown that the clustering of multiple viral envelopes is needed for IAV entry, suggesting that this activity may be hindered by IFITMs residing in the host-derived viral and/or host membranes (Ivanovic et al., 2013). Second, IFITM homo- and heteromers within the membrane may stabilize membrane complexes by inhibiting dissociation, i.e., stabilizing the vacuolar ATPase may increase endosomal acidity and potentially salinity (Wee et al., 2012). Third, the insertions of each IFITM's IM domains into the cytosolic-facing leaflet of the membrane may produce a positive curvature in the bilayer as well described for other membrane-associated proteins (Callan-Jones and Bassereau, 2012; Nikolaus and Herrmann, 2012; Voeltz et al., 2006; Yount et al., 2012). Therefore, by producing a concave and rigid membrane, the IFITM proteins may create a barrier for the viral fusion machinery. Notably, using such a general strategy to protect oneself from many viruses would produce multiple fitness advantages.

Given these models of IFITM3-mediated restriction, we favor a scenario wherein AmphoB rescues IAV replication by increasing membrane fluidity and planarity; this would permit viral-host receptor interactions and pore formation. In support of this notion, it has been reported that AmphoB enhances membrane fluidity (Abu-Salah, 1991; Henry-Toulmé et al., 1989;Younsi et al., 2000). As mentioned, AmphoB first binds to cholesterol in the lipid bilayer and then forms transmembrane pores. A more cationic analog of AmphoB, DS-AmpB-020, was more potent against IFITM3, which likely arises from its improved hydrogen-bonding ability, which could augment either channel formation or interactions with negatively charged phospholipids to increase membrane fluidity. We have shown that blocking pore conductance does not alter AmphoB's effects on restriction. Therefore, fenestration of the lipid bilayer by pores formed by either AmphoB or DS-AmpB-020 may be increasing membrane fluidity. In addition, the presence of these heptaenes in the membrane may disrupt cholesterol-phospholipid interactions and/or IFITM interactions, leading to increased membrane flexibility (Figure 6F). In support of this last assertion, we found that adding additional cholesterol reduced by the half the alleviation of IFITM3 restriction by AmphoB.

We note, however, that AmphoB did little to alleviate either IFITM1's antiviral action or it's inhibitory effect on membrane fluidity and cell-to-cell fusion. Therefore, additional efforts will be needed to determine if the effect of IFITM1 on plasma membrane fluidity is the same as the effect of IFITM3 on endosomal membranes and if AmphoB's antagonism of IFITM3 results from alterations in membrane fluidity. In this regard, we are unsure as to why AmphoB specifically overcomes IFITM2 and IFITM3 while leaving IFITM1's actions predominantly extant. One factor may be proximity, because AmphoB is endocytosed quite rapidly leading to its concentration in the late endosomes and lysosomes, the areas of IFITM3's highest concentrations. Future studies using derivatives of AmphoB and IFITM mutant proteins will be useful in further testing such models.

Intrigued by recent reports, we tested the role of VAPA, cholesterol, and oleic acid in IFITM3-mediated restriction. Overexpression of VAPA modestly decreased IFITM3-mediated restriction of IAV in our assays. Based on our use of the same

(F) Whole cell lysates from the indicated cells in (E) were subjected to immunoblotting using the indicated antibodies. Actin serves as a loading control.
(G) Niemann-Pick type c1 (NPC) or wild-type (WT) primary human fibroblasts infected with the indicated IAVs with or without AmphoB (Ampho) treatment.
(H) Confocal images of primary human fibroblasts in (G) stained with filipin (white) to detect cholesterol and immunostained for LAMP1 (red) to identify the late endosomal and lysosomal compartments. Scale bar = 15 μM.

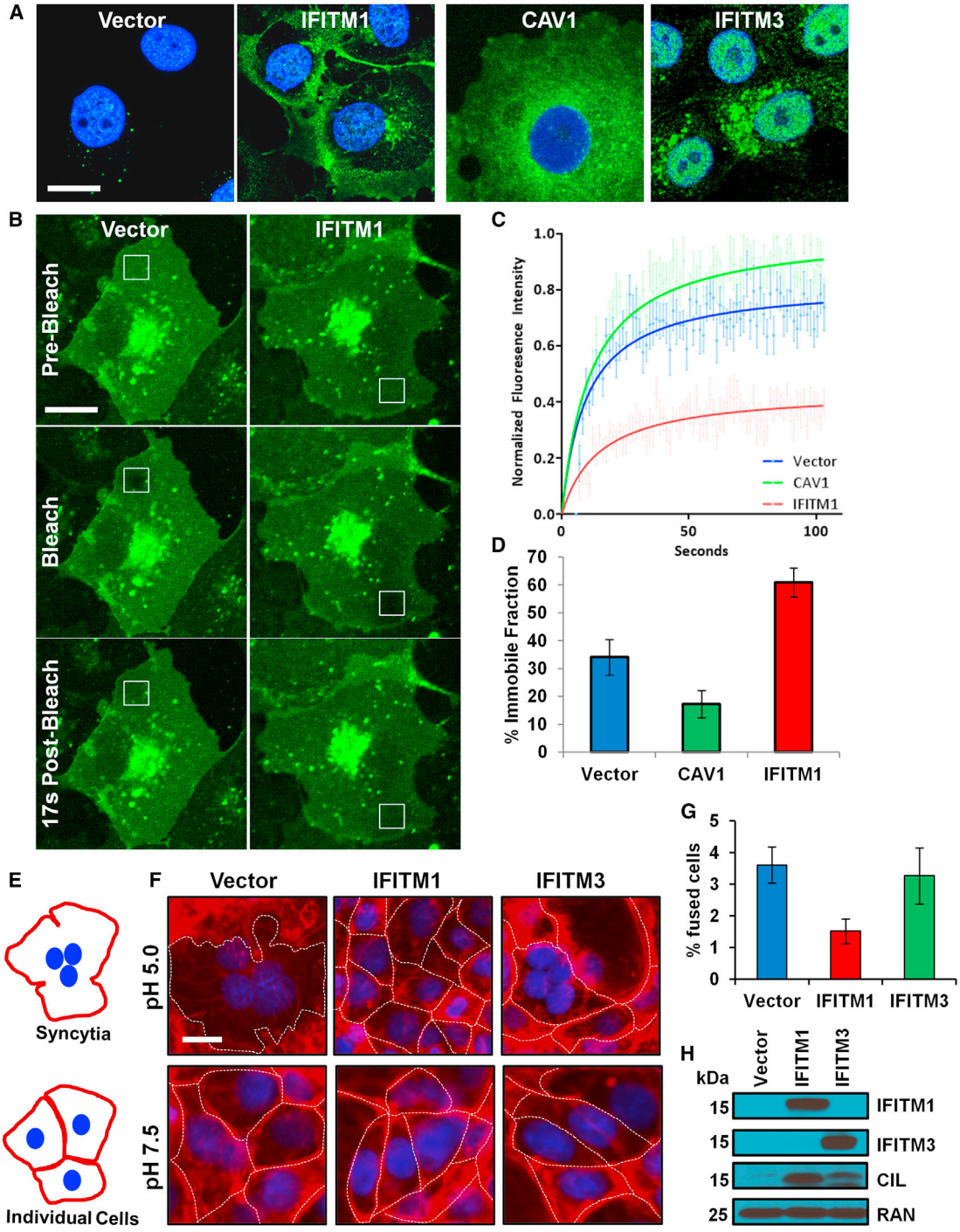

Figure 5. IFITM1 Decreases Membrane Fluidity and Inhibits Cell-to-Cell Fusion

(A) COS-7 cells were stably transduced with retroviruses expressing the empty vector (Vector), IFITM1, CAV1-teal fluorescence protein (TFP), or IFITM3. Cells were then confocally imaged to detect the expressed proteins (all in green; additional specificity control images in Figure S4A). Nuclear DNA was stained with DAPI (blue). Scale bar, 10 μM.

(B) Fluorescence recovery after photobleaching of the plasma membrane. COS7-vector or COS7-IFITM1 cells were stained with DiO and the unbound dye removed. Cells were photobleached in the indicated area (white square) with a 488 laser, and a series of pictures out to 95 s postbleach were taken. Images are shown for prebleach, postbleach, and 17 s postbleach ($t^{1/2}$ of IFITM1 recovery).

(C) COS7-vector, COS7-CAV1, or COS7-IFITM1 cell fluorescence recovery was quantified using Leica Lite software, with each individual time point representing the average of ten normalized readouts. PRISM software was then used to plot the best-fit exponential decay line. Results are representative of three independent experiments.

(legend continued on next page)

cell line, A549, and antibody against VAPA as the seminal report, we estimate that our overexpression of VAPA met or surpassed the published levels. Modulation of cholesterol levels had no appreciable effect on IFITM3-mediated restriction, suggesting that cholesterol mislocalization does not contribute to VAPA's antagonism of IFITM3. Furthermore, cells expressing either of three IFITM3 proteins containing mutations that span IM2, the reported interaction domain of IFITM3 with VAPA, exhibited WT levels of restriction and intracellular cholesterol. These results suggest that a direct interaction between VAPA and IFITM3 does not underlie the subtle effect of VAPA on restriction. We mention, however, that our alanine scanning strategy may have been too conservative because IM2 is a hydrophobic domain. We also addressed the role of oleic acid in overcoming IFITM-mediated inhibition of cell-to-cell fusion. Specifically, we found that oleic acid cannot overcome IFITM1- or IFITM3-mediated restriction of IAV in vitro under the conditions tested. Furthermore, oleic acid did not overcome IFITM1-mediated inhibition of cell-to-cell fusion assays by IAV particles (data not shown). Therefore, while these recent reports have improved our understanding of IFITM3-mediated restriction, we conclude that additional mechanistic studies are required.

When we found that AmphoB prevented IFITM3's antiviral actions, it suggested that patients treated with AmphoB formulations might be at greater risk for influenza (Everitt et al., 2012). Therefore, we tested a clinical preparation of AmphoB, AmBisome, in vivo and found that similar to *Ifitm3*$^{-/-}$ mice, WT littermates treated with AmBisome developed severe illness from a normally nonpathogenic IAV strain. Individuals with a variant of IFITM3 are more likely to be hospitalized with influenza, suggesting that IFITM3 plays a role in protecting human populations (Everitt et al., 2012); indeed, this IFITM3 allele (rs12254-C) was recently reported to convey a large population-attributable risk of 54.25% in the Chinese population (Zhang et al., 2013). Moreover, IFITM3 is critical for protecting CD8^{+} resident memory T cell populations during IAV infections in vivo, arguing that AmphoB's antagonism of IFITM3 may impair the adaptive immune system as well (Wakim et al., 2013). Collectively, these data suggest that patients receiving antifungal therapy with liposomal AmphoB may be functionally immunosuppressed and therefore more vulnerable to influenza. Many patients receiving AmBisome have lost their adaptive and innate immune defenses, so the role of intrinsic immune factors may be critical in protecting them against IAV (Moen et al., 2009). In addition, some of these patients are also on prophylactic AmBisome therapy and so may potentially be incurring greater IAV infection risks. It is our hope that the reporting of the mechanism and the in vivo consequences of this interaction between IFITM3 and amphotericin B may help stimulate translational studies and potentially guide patient care.

EXPERIMENTAL PROCEDURES

Tetraethylammonium and Acetylcholine Experiment

Tetraethylammonium (TEA, 5 μM, Sigma) and acetylcholine (ACh, 5 μM, Sigma) were incubated with A549 cells with or without 1 μM of AmphoB at 37°C for 1 hr. prior to infection with WSN/33. After infection, cells were incubated at 37°C for 12 hr. then fixed and analyzed as described previously.

NP and Acid-Induced HA Translocation Experiments and Confocal Imaging

Experiments for detection of NP nuclear translocation or acid-induced HA conformational change were modified from previously described experiments (Feeley et al., 2011). Nuclear translocation of vRNP was quantified by analyzing images using Imaris 7.1 (Bitplane scientific software) as previously described.

Cell-to-Cell Fusion Assay

Vector, IFITM1, or IFITM3 COS-7 cells and PR8 virus were chilled on ice before the addition of virus to cells (White et al., 1981, 1982). Virus and cells were incubated at 4°C for 40 min. Cells were then rinsed and incubated with 37°C pH 5.0 or pH 7.5 buffer (10 mM of MES and 10 mM of HEPES in 1× PBS) for 5 min. Subsequently, the buffers were replaced with warm media and the cells incubated in a 37°C incubator for an additional 5 hr. Cells were then fixed with 4% paraformaldehyde, permeabilized with 0.2% Triton X-100, and stained with Alexa Fluor 594-conjugated phalloidin (1:500, Life Technologies) and Hoechst 33342 (1:10,000, Invitrogen) before imaging. Fusion events were identified based on the formation of syncytia and nuclear aggregation. The percentage of fusion was calculated using a ratio of the nuclei within fused cells over the total nuclei for each microscopic field evaluated with more than five fields examined for each experimental condition.

FRAP

Cells were plated on glass-bottom 6c m dishes (MatTek) 16 hr prior to analysis. Cells were pretreated with fresh media or fresh media containing 1 μM of AmphoB for 1 hr then stained with Vibrant DiI or DiO (Invitrogen) for 15 min at 37°C, then washed with 1× PBS twice. FRAP was then done on the cells using a Leica SP5 with the Leica FRAP wizard. At least ten cells were measured per experiment, and LAS AF Lite (Leica) software was used to quantify the intensity of the photobleached area, the total cell fluorescence, and an area outside of the cells for normalization. The normalized intensities of the photobleached areas were then averaged together to form a representative curve of each condition.

Live Cell Imaging

Cells were plated onto chambered coverglass slides (Thermo Fisher Scientific) and cultured overnight. Before imaging, cells were incubated at 37°C for 1 hr with 5 μM of yellow/blue dextran (Life Technologies, 10,000 MW, L-22460) or 5 μM of Asante sodium green (TefLabs) in the presence or absence of 1 μM of

(D) The COS7-vector, COS7-CAV1, or COS7-IFITM1 percent immobile fraction was calculated by first subtracting the normalized average of the 95 s postbleach images, then subtracting those values from 1 to determine the amount of membrane that did not recover. Results are representative of three independent experiments.

(E) Schematic of IAV-induced cell-to-cell fusion assay. Individual cells (lower portion) exhibit distinct boundaries of actin (red lines) and clearly spaced nuclei (blue ovals). By comparison, after incubation with IAV and the addition of pH 5.0 buffer, the individual cells fuse and form syncytia, which possess multiple clustered nuclei with no intervening actin boundaries.

(F) IAV-induced cell-to-cell fusion assay. Chilled IAV (PR8, moi 500–1,000) was incubated with the indicated stably transduced COS-7 cell lines from (A). Warm buffer of either pH 5.0 or 7.5 was added, followed by warm media. Cells were incubated for 5 hr and then fixed and stained to monitor fusion events for both actin (phalloidin, red), to highlight cellular boundaries (white dashed lines), and DNA (blue), to detect closely clustered nuclei present in syncytia. Scale bar, 10 μm.

(G) Percentage of fused cells in experiments using pH 5.0 buffer in (F). Fusion events per 100 nuclei were calculated and values represent the average of three to five images from each of three independent experiments ± SD.

(H) Immunoblot of the indicated cell lines from (A). The CIL antisera recognize an epitope that is identical in both IFITM1 and IFITM3.

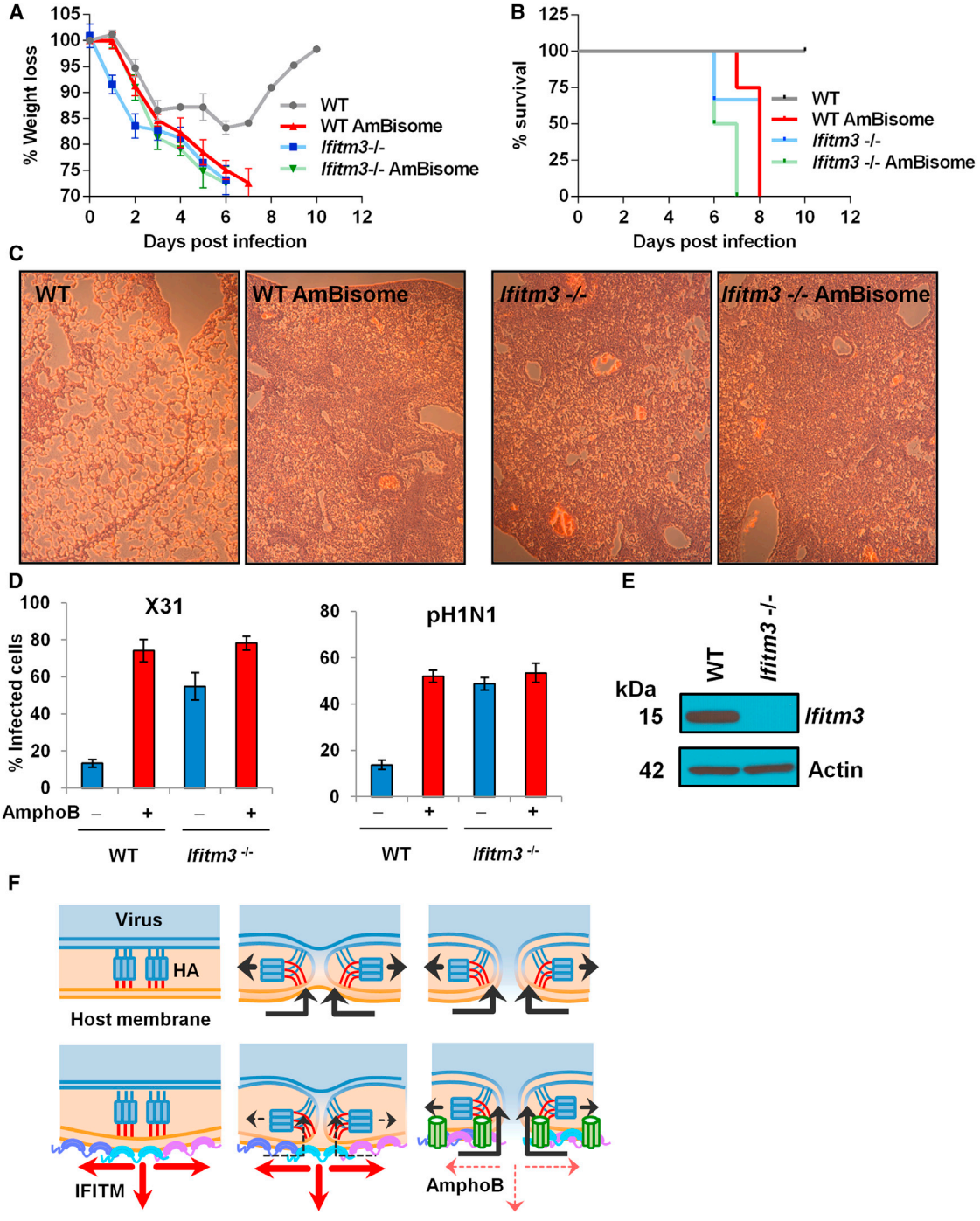

Figure 6. AmBisome Increases Influenza Morbidity and Mortality

(A and B) Change in body mass (A) and survival (B) of WT and *Ifitm3*$^{-/-}$ mice with or without intravenous administration of AmBisome (3 mg/kg) on days 0, 2, and 4 relative to intranasal inoculation with IAV X-31 (10,000 pfu); n > 3.

(C) WT and *Ifitm3*$^{-/-}$ mice were treated or not treated with AmBisome and then challenged with X-31 influenza as above. At day 6 postinfection, lung sections were prepared and stained with hematoxylin and eosin.

(D) The indicated MEFs were incubated for 1 hr in the presence (red, +) or absence (blue, –) of 1 μM AmphoB and then challenged with X-31 or pandemic A/California/7/2009 (pH1N1) followed by fixation and immunostaining for NP. Numbers represent the mean percentage of infected cells of three separate experiments ± SD.

(E) Immunoblot of the indicated cell lines from (D).

(F) Model of IFITMs inhibiting viral fusion. Top panels depict HA-directed membrane fusion. Insertion of the viral fusion peptide (red) by the HA protein into the host's endosomal membrane is followed by an acid-induced conformational change in HA producing a hemifusion transition state (middle, arrows represent force

(legend continued on next page)

AmphoB, 5 μM of ionophores, or 1 μM of AmphoB ± TEA or ACh. Cells were then visualized with confocal microscopy. For the ratiometric dextran experiments, we calculated the average ratios of pH-sensitive dextran signal to pH-insensitive dextran signal in the RAB7-RFP compartment normalized to this same ratio as determined for the vector-RAB7-RFP control cells.

Mouse Infection

Background-matched wild-type (>95% C57BL/6) and Ifitm3$^{-/-}$ mice (Everitt et al., 2012) 8 to10 weeks of age were maintained in accordance with UK Home Office regulations, UK Animals Scientific Procedures Act 1986 under the project license PPL80/2099 (Everitt et al., 2012). This license was reviewed by The Wellcome Trust Sanger Institute Ethical Review Committee. Groups of more than five isoflurane-anaesthetized mice of both genotype were intranasally inoculated with 1 × 10^4 plaque-forming units of X-31 influenza in 50 μl of sterile PBS (Everitt et al., 2012). On days 0, 2, and 4, the AmBisome-treated mice (wild-type or matched Ifitm3$^{-/-}$) were administered 3 mg/kg of AmBisome (Gilead) intravenously. Their weight was recorded daily and they were monitored for signs of illness. Mice exceeding 25% total weight loss were euthanized in accordance with UK Home Office guidelines. Littermate controls were used in all experiments.

SUPPLEMENTAL INFORMATION

Supplemental information includes Supplemental Experimental Procedures and five figures and can be found with this article online at http://dx.doi.org/10.1016/j.celrep.2013.10.033.

ACKNOWLEDGMENTS

We thank University of Massachusetts Medical School (UMMS) colleagues R. Fish, B. Hobbs, L. Benson, T. Brailey, and J. Barrett and Ragon Institute colleagues M. Boyarina, K. Donnelly, and P. Richtmeyer. We thank A.T. Chan (Massachusetts General Hospital), A. Quaresma and J. Nickerson (UMMS), J. White (University of Virginia), K. Weninger (North Carolina State University), and G. Melikian (Emory University) for helpful discussions and advice. This work was generously supported by a grant (1R01AI091786) from the National Institute of Allergy and Infectious Diseases of the National Institutes of Health (to A.L.B.). A.L.B. is grateful to the Charles H. Hood Foundation, the Burroughs Wellcome Fund, the Bill and Melinda Gates Foundation, the Phillip T. and Susan M. Ragon Foundation, and the Harvard and UMMS Centers for AIDS Research for their generous support. P.K, S.C., and A.R.E are supported by the Wellcome Trust. S.J.E. is a Howard Hughes Investigator.

Received: February 12, 2013
Revised: September 23, 2013
Accepted: October 21, 2013
Published: November 21, 2013

REFERENCES

Abu-Salah, K.M. (1991). Perturbation of the fluidity of the erythrocyte membrane with ionophoric antibiotics and lipophilic anaesthetics. Biochem. Pharmacol. *42*, 1947–1951.

Amini-Bavil-Olyaee, S., Choi, Y.J., Lee, J.H., Shi, M., Huang, I.C., Farzan, M., and Jung, J.U. (2013). The antiviral effector IFITM3 disrupts intracellular cholesterol homeostasis to block viral entry. Cell Host Microbe *13*, 452–464.

Bailey, C.C., Huang, I.C., Kam, C., and Farzan, M. (2012). Ifitm3 limits the severity of acute influenza in mice. PLoS Pathog. *8*, e1002909.

Bellmann, R. (2007). Clinical pharmacokinetics of systemically administered antimycotics. Curr. Clin. Pharmacol. *2*, 37–58.

Bolard, J. (1986). How do the polyene macrolide antibiotics affect the cellular membrane properties? Biochim. Biophys. Acta *864*, 257–304.

Brass, A.L., Huang, I.C., Benita, Y., John, S.P., Krishnan, M.N., Feeley, E.M., Ryan, B.J., Weyer, J.L., van der Weyden, L., Fikrig, E., et al. (2009). The IFITM proteins mediate cellular resistance to influenza A H1N1 virus, West Nile virus, and dengue virus. Cell *139*, 1243–1254.

Brutyan, R.A., and McPhie, P. (1996). On the one-sided action of amphotericin B on lipid bilayer membranes. J. Gen. Physiol. *107*, 69–78.

Cai, C., Zhu, H., and Chen, J. (2004). Overexpression of caveolin-1 increases plasma membrane fluidity and reduces P-glycoprotein function in Hs578T/Dox. Biochem. Biophys. Res. Commun. *320*, 868–874.

Callan-Jones, A., and Bassereau, P. (2012). Membrane fission: curvature-sensitive proteins cut it both ways. Dev. Cell *22*, 691–692.

Cybulska, B., Bolard, J., Seksek, O., Czerwinski, A., and Borowski, E. (1995). Identification of the structural elements of amphotericin B and other polyene macrolide antibiotics of the hepteane group influencing the ionic selectivity of the permeability pathways formed in the red cell membrane. Biochim. Biophys. Acta *1240*, 167–178.

Diamond, M.S., and Farzan, M. (2013). The broad-spectrum antiviral functions of IFIT and IFITM proteins. Nat. Rev. Immunol. *13*, 46–57.

Everitt, A.R., Clare, S., Pertel, T., John, S.P., Wash, R.S., Smith, S.E., Chin, C.R., Feeley, E.M., Sims, J.S., Adams, D.J., et al.; GenISIS Investigators; MOSAIC Investigators (2012). IFITM3 restricts the morbidity and mortality associated with influenza. Nature *484*, 519–523.

Feeley, E.M., Sims, J.S., John, S.P., Chin, C.R., Pertel, T., Chen, L.M., Gaiha, G.D., Ryan, B.J., Donis, R.O., Elledge, S.J., and Brass, A.L. (2011). IFITM3 inhibits influenza A virus infection by preventing cytosolic entry. PLoS Pathog. *7*, e1002337.

Hartsel, S.C., Benz, S.K., Ayenew, W., and Bolard, J. (1994). Na+, K+ and Cl- selectivity of the permeability pathways induced through sterol-containing membrane vesicles by amphotericin B and other polyene antibiotics. Eur. Biophys. J. *23*, 125–132.

Helenius, A., Kielian, M., Wellsteed, J., Mellman, I., and Rudnick, G. (1985). Effects of monovalent cations on Semliki Forest virus entry into BHK-21 cells. J. Biol. Chem. *260*, 5691–5697.

Henry-Toulmé, N., Sarthou, P., Seman, M., and Bolard, J. (1989). Membrane effects of the polyene antibiotic amphotericin B and of some of its derivatives on lymphocytes. Mol. Cell. Biochem. *91*, 39–44.

Hoop, C.L., Sivanandam, V.N., Kodali, R., Srnec, M.N., and van der Wel, P.C. (2012). Structural characterization of the caveolin scaffolding domain in association with cholesterol-rich membranes. Biochemistry *51*, 90–99.

Huang, I.C., Bailey, C.C., Weyer, J.L., Radoshitzky, S.R., Becker, M.M., Chiang, J.J., Brass, A.L., Ahmed, A.A., Chi, X., Dong, L., et al. (2011). Distinct patterns of IFITM-mediated restriction of filoviruses, SARS coronavirus, and influenza A virus. PLoS Pathog. *7*, e1001258.

Ivanovic, T., Choi, J.L., Whelan, S.P., van Oijen, A.M., and Harrison, S.C. (2013). Influenza-virus membrane fusion by cooperative fold-back of stochastically induced hemagglutinin intermediates. eLife *2*, e00333.

Jiang, D., Weidner, J.M., Qing, M., Pan, X.B., Guo, H., Xu, C., Zhang, X., Birk, A., Chang, J., Shi, P.Y., et al. (2010). Identification of five interferon-induced cellular proteins that inhibit west nile virus and dengue virus infections. J. Virol. *84*, 8332–8341.

John, S.P., Chin, C.R., Perreira, J.M., Feeley, E.M., Aker, A.M., Savidis, G., Smith, S.E., Elia, A.E., Everitt, A.R., Vora, M., et al. (2013). The CD225 domain

vectors), followed by a fusion pore (right). Arrows represent force vectors throughout. We postulate that IFITM proteins prevent fusion pore formation (bottom panels); situated within the cytosolic-facing leaflet, multiple interacting IFITM proteins act as reinforcing bars to decrease membrane flexibility and prevent the viral fusion machinery from distending the host membrane (red arrows). The intramembrane insertions of each IFITM into the cytosolic leaflet also inhibit fusion by producing a membrane curvature away from the viral fusion machinery. AmphoB (green, rightmost lower panel) is postulated to rescue IAV replication by increasing membrane fluidity and planarity, thereby permitting fusion pore formation.

of IFITM3 is required for both IFITM protein association and inhibition of influenza A virus and dengue virus replication. J. Virol. *87*, 7837–7852.

Li, K., Markosyan, R.M., Zheng, Y.M., Golfetto, O., Bungart, B., Li, M., Ding, S., He, Y., Liang, C., Lee, J.C., et al. (2013). IFITM proteins restrict viral membrane hemifusion. PLoS Pathog. *9*, e1003124.

Medina, R.A., and García-Sastre, A. (2011). Influenza A viruses: new research developments. Nat. Rev. Microbiol. *9*, 590–603.

Moen, M.D., Lyseng-Williamson, K.A., and Scott, L.J. (2009). Liposomal amphotericin B: a review of its use as empirical therapy in febrile neutropenia and in the treatment of invasive fungal infections. Drugs *69*, 361–392.

Mudhasani, R., Tran, J.P., Retterer, C., Radoshitzky, S.R., Kota, K.P., Altamura, L.A., Smith, J.M., Packard, B.Z., Kuhn, J.H., Costantino, J., et al. (2013). IFITM-2 and IFITM-3 but not IFITM-1 restrict Rift Valley fever virus. J. Virol. *87*, 8451–8464.

Nikolaus, J., and Herrmann, A. (2012). Functional relevance of transmembrane domains in membrane fusion. Biol. Chem. *393*, 1231–1245.

Paquet, V., Volmer, A.A., and Carreira, E.M. (2008). Synthesis and in vitro biological properties of novel cationic derivatives of amphotericin B. Chemistry *14*, 2465–2481.

Perreira, J.M., Chin, C.R., Feeley, E.M., and Brass, A.L. (2013). IFITMs restrict the replication of multiple pathogenic viruses. J. Mol. Biol. Published online September 25, 2013. http://dx.doi.org/10.1016/j.jmb.2013.09.024.

Rawat, S.S., Zimmerman, C., Johnson, B.T., Cho, E., Lockett, S.J., Blumenthal, R., and Puri, A. (2008). Restricted lateral mobility of plasma membrane CD4 impairs HIV-1 envelope glycoprotein mediated fusion. Mol. Membr. Biol. *25*, 83–94.

Roethl, E., Gassner, M., Krenn, B.M., Romanovskaya-Romanko, E.A., Seper, H., Romanova, J., Nakowitsch, S., Sturlan, S., Wolschek, M., Sirotkin, A., et al. (2011). Antimycotic-antibiotic amphotericin B promotes influenza virus replication in cell culture. J. Virol. *85*, 11139–11145.

Schoggins, J.W., Wilson, S.J., Panis, M., Murphy, M.Y., Jones, C.T., Bieniasz, P., and Rice, C.M. (2011). A diverse range of gene products are effectors of the type I interferon antiviral response. Nature *472*, 481–485.

Scott, C.C., and Gruenberg, J. (2011). Ion flux and the function of endosomes and lysosomes: pH is just the start: the flux of ions across endosomal membranes influences endosome function not only through regulation of the luminal pH. Bioessays *33*, 103–110.

Terazima, E., and Yoshino, M. (2010). Modulatory action of acetylcholine on the Na+-dependent action potentials in Kenyon cells isolated from the mushroom body of the cricket brain. J. Insect Physiol. *56*, 1746–1754.

Voeltz, G.K., Prinz, W.A., Shibata, Y., Rist, J.M., and Rapoport, T.A. (2006). A class of membrane proteins shaping the tubular endoplasmic reticulum. Cell *124*, 573–586.

Volmer, A.A., and Carreira, E.M. (2010). Active amphotericin B derivatives position the mycosamine in two radial orientations. Chembiochem *11*, 778–781.

Wakim, L.M., Gupta, N., Mintern, J.D., and Villadangos, J.A. (2013). Enhanced survival of lung tissue-resident memory CD8(+) T cells during infection with influenza virus due to selective expression of IFITM3. Nat. Immunol. *14*, 238–245.

Wee, Y.S., Roundy, K.M., Weis, J.J., and Weis, J.H. (2012). Interferon-inducible transmembrane proteins of the innate immune response act as membrane organizers by influencing clathrin and v-ATPase localization and function. Innate Immun. *18*, 834–845.

Weidner, J.M., Jiang, D., Pan, X.B., Chang, J., Block, T.M., and Guo, J.T. (2010). Interferon-induced cell membrane proteins, IFITM3 and tetherin, inhibit vesicular stomatitis virus infection via distinct mechanisms. J. Virol. *84*, 12646–12657.

White, J., Matlin, K., and Helenius, A. (1981). Cell fusion by Semliki Forest, influenza, and vesicular stomatitis viruses. J. Cell Biol. *89*, 674–679.

White, J., Helenius, A., and Gething, M.J. (1982). Haemagglutinin of influenza virus expressed from a cloned gene promotes membrane fusion. Nature *300*, 658–659.

Wilkins, C., Woodward, J., Lau, D.T., Barnes, A., Joyce, M., McFarlane, N., McKeating, J.A., Tyrrell, D.L., and Gale, M., Jr. (2013). IFITM1 is a tight junction protein that inhibits hepatitis C virus entry. Hepatology *57*, 461–469.

Wyles, J.P., McMaster, C.R., and Ridgway, N.D. (2002). Vesicle-associated membrane protein-associated protein-A (VAP-A) interacts with the oxysterol-binding protein to modify export from the endoplasmic reticulum. J. Biol. Chem. *277*, 29908–29918.

Younsi, M., Ramanandraibe, E., Bonaly, R., Donner, M., and Coulon, J. (2000). Amphotericin B resistance and membrane fluidity in Kluyveromyces lactis strains. Antimicrob. Agents Chemother. *44*, 1911–1916.

Yount, J.S., Karssemeijer, R.A., and Hang, H.C. (2012). S-palmitoylation and ubiquitination differentially regulate interferon-induced transmembrane protein 3 (IFITM3)-mediated resistance to influenza virus. J. Biol. Chem. *287*, 19631–19641.

Zhang, Y.H., Zhao, Y., Li, N., Peng, Y.-C., Giannoulatou, E., Jin, R.-H., Yan, H.-P., Wu, H., Liu, J.-H., Liu, N., et al. (2013). Interferon-induced transmembrane protein-3 genetic variant rs12252-C is associated with severe influenza in Chinese individuals. Nat. Commun. *4*, 1418.